Boiling heat transfer on a dendritic and microporous surface in R134a and FC-72

Richard Furberg, Bjorn Palm

Accepted Manuscript

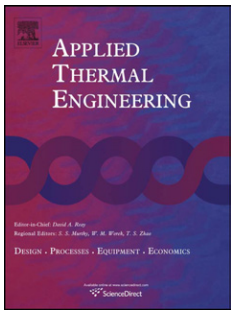

Title: Boiling heat transfer on a dendritic and microporous surface in R134a and FC-72

Authors: Richard Furberg, Bjorn Palm

PII: S1359-4311(11)00386-3

DOI: 10.1016/j.applthermaleng.2011.07.027

Reference: ATE 3654

To appear in: *Applied Thermal Engineering*

Received Date: 16 February 2011

Revised Date: 15 July 2011

Accepted Date: 16 July 2011

Please cite this article as: R. Furberg, B. Palm. Boiling heat transfer on a dendritic and microporous surface in R134a and FC-72, Applied Thermal Engineering (2011), doi: 10.1016/j.applthermaleng.2011.07.027

Boiling heat transfer on a dendritic and microporous surface in R134a and FC-72

Richard Furberg* and Björn Palm
Royal Institute of Technology, Sweden (KTH)
School of Industrial Engineering and Management (ITM)
Department of Applied Thermodynamics and Refrigeration (EGI)
Brinellvägen 68, 10044, Stockholm, Sweden
* Corresponding author, tel: +46-707339783, e-mail: richard.furberg@energy.kth.se

ABSTRACT

A visualization study was conducted with the aim of deepening the understanding of the boiling mechanism in a dendritic and microporous copper structure for enhanced boiling heat transfer. The unique structure has earlier been shown to enhance heat transfer in pool boiling applications as well as in convective boiling in both small and large channels. Pool boiling tests were conducted in R134a and in the dielectric fluid FC-72 and were visualized with a high speed imaging system. Data on bubble size, bubble frequency density, heat transfer coefficient and the latent and sensible heat flux contributions were collected and calculated at heat flux varying between 2 and 15 W/cm^2. The enhanced surface produces smaller bubbles and sustains a high bubble frequency density in both fluids, even at low heat flux. An enhanced latent heat transfer mechanism of up to 10 times, compared to that of a plain reference surface, is the main reason for the improved boiling heat transfer performance on the enhanced surface. The data also suggests that the high nucleation bubble frequency density leads to increased bubble pumping action and thus enhancing single phase convection of up to 6 times. The results in this study highlight the importance of both two and single-phase heat transfer within the porous structure.

KEYWORDS

Enhanced Boiling; Pool Boiling: Porous media; Boiling Mechanism; R134A; FC-72

NOMENCLATURE

A	apparent heat transfer area [m^2]
c_p	specific heat of liquid at constant pressure [J/(kgK]
d	bubble diameter [m]
d_{avg}	average frequency weighted bubble diameter [m]
D	depth of the boiling surface [m]
f	bubble frequency for each bubble in the analyzed image [s^{-1}]
H	height of test object
h	heat transfer coefficient [W/(mK)]
h_{fg}	enthalpy of vaporization [J/kg]
L	length of boiling surface [m]
L_{window}	length of the analyzed section [m]
$n\mu p$	dendritic and microporous copper surface
q''	heat flux [W/m^2]
Q'	heat flow rate [W]
Q'_{lat}	total latent heat [W]
T_s	surface temperature [°C]
T_{liq}	liquid temperature [°C]
V	bubble volume [m^3]
V'	vapor volume flow rate for a bubble [m^3/s]
w	width of boiling surface [m]
x	quality [-]

ρ_{liq}	liquid density [kg/m^3]
$\rho_{sat,x=1}$	vapor saturation density [kg/m^3]
τ	time for bubble to move through the analyzed section [s]
ΔT	temperature difference [K]

Subscripts

avg	average
i	bubble index
lat	latent
liq	liquid
nμp	dendritic and microporous surface
ref	reference surface
sat	saturated
sens	sensible
tot	total

1. INTRODUCTION

The widespread occurrence of boiling heat transfer in refrigeration and air conditioning equipment and in high heat flux applications, such as in the cooling of electronic components and fuel rods, have been important motives for researchers to deepen the understanding of nucleate and convective boiling. The use of high resolution experimental techniques, for instance: micro fabricated heater devices with integrated temperature sensors, micro-heater arrays and high speed infrared cameras by researchers such as Stephan and Kern [1], Demiray and Kim [2], Moghaddam and Kiger [3] have been of great importance to recent advancements in the understanding of the mechanisms of nucleate boiling heat transfer. These studies have been able to discern and quantify the effect and interactions of different heat transfer mechanisms, such as; transient conduction, single phase micro convection and micro-layer evaporation and have therefore contributed greatly to the understanding of the boiling phenomenon. Studies of the fundamentals of pool boiling have typically been conducted on single bubbles and on very smooth surfaces, such as atomically smooth silicone. These simplified conditions and surfaces are significantly different from that of boiling surfaces that are fabricated with various features that have been found to enhance boiling heat transfer mechanisms.

The pool boiling mechanisms in enhanced surfaces with machined structures have been best understood, since they are conducive to parameter variation and with features large enough to facilitate imaging rather easily. Dynamic explanation modeling of these structures was pioneered by Nakayama et al. [4] and further developed by many others, such as Chien and Webb [5] and Ramaswamy et al. [6] and has increased the understanding of possible enhancement mechanisms, such as meniscus evaporation and internal evaporation. Li and Peterson [7] fabricated porous surfaces out of sintered copper wire mesh, and found that the mechanisms of improvement are mainly thought to be due to the augmentation of the wetted area, the number of nucleation sites, the intensified interaction among bubbles, as well as film and capillary evaporation induced through the use of porous coatings. Porous coatings with higher thermal conductivity were found to perform better than those with lower thermal conductivities, especially at low heat fluxes. Layers of porous particles have also been studied rather extensively by authors such as Kim et al.[8] and Hwang and Kaviany [9], improving the understanding of heat transfer in these structures.

In general, heat is transferred from the boiling surface as sensible and latent heat, often referred to as single and two-phase convection. Single phase convection is influenced by natural convection on the surface, due to density differences in the liquid, as well as the liquid motion caused by growing and departing bubbles. The mechanisms driving the latent heat transfer take place around the liquid-, vapor- and surface interface of the growing vapor bubbles. All of these modes of heat transfer may be affected by different enhanced surfaces. In this study, detailed heat transfer and bubble data has been gathered and analyzed, with the aim of deepening the understanding of the boiling mechanism in a unique nano- and micro-porous copper structure (nμp) used to enhance boiling, previously reported on by Furberg et al.[10, 11] and later by El-Genk and Ali [12]. The studied structure has earlier been shown to enhance boiling of R134a in pool- and convective boiling applications in both small and large channels, as reported by Furberg et al. [13, 14]. In an effort to gain more insight into the enhancement mechanisms of the dendritic and micro-porous structure, pool boiling tests were conducted in FC-72 and R134a, visualized with a high speed imaging system.

2. EXPERIMENTAL APPARATUS AND PROCEDURE

2.1 Experimental Set-up

Figure 1 shows the experimental pool boiling set-up and its most important components. The stainless steel chamber was insulated with 10 mm thick foam insulation and had an internal volume of about 3 dm^3. The signal from a pressure transducer, measuring the vapor pressure of the boiling chamber, was used to regulate the condenser effect, in order to maintain constant pressure in the boiling chamber. The condenser consisted of a water cooled tube, where the water flow rate, and thus indirectly the system's pressure, was controlled with a DC pump. The cooling water was in turn cooled by a compressor driven cooling unit. With this set-up, the desired pressure level could be maintained within a range of ±2 mbar during the test runs. An auxiliary cartridge heater was installed into the boiling chamber to maintain the bulk liquid at saturated conditions and to provide some agitation during the degassing process prior to testing of FC-72. The heat load from the auxiliary heater was also needed to balance the condenser cooling power, since the heat input to the test section was relatively small. The liquid level was kept at about 5 cm above the test section for all tests to assure reproducible test conditions. A thermocouple (type T) was employed to measure the liquid temperature and was placed about 10 mm above the test section. The pressure transducer, thermocouples and the DC power supply were connected to data-logger (Agilent 34970A), which in turn was connected to a PC.

Two large sight glasses (100 mm diam.) on either side of the boiling chamber facilitated the use of a high speed video camera (Redlake, MotionXtra, HG-LE) with a Navitar 12x macro zoom lens. Films were taken at 1000 fps and two 250W tungsten lamps (Dedocool Dedolight) were used as light sources. For bubble measurements, the light was directed into the camera to create a sharp bubble contrast, while for boiling surface observations, the lights were directed onto the boiling surface. All film parameters, such as frames per second, shutter speed and length of film sequence were controlled by, processed and stored in a PC.

2.2 Test Object

The test object consisted of a pyramid like machine milled copper piece, encased in epoxy and Teflon for insulation, as seen in Figure 2. The length (L) of the boiling surface was 15 mm, but its width (w) only about 1 mm to facilitate the filming of departing bubbles. The heater was fabricated from coiled Ni-Chrome wire that was attached to the bottom side of the test object, using high temperature resistant cement. A thin layer of cement at the backside of the test object electrically insulated the wire from the copper. A DC power supply was used to generate a current through the heater. Two thermocouples (type T) were used to measure the temperature of the boiling surface, located in 0.6 mm inner diameter and 5 mm deep holes on both sides of the test object and 2 mm below the surface. Before insertion, the tip of each thermocouple was coated in silver epoxy (Circuitworks, CW2400) to assure good thermal contact. An epoxy filler was used to cover most of the test object, while a liquid rubber gasket seal (Sealtite) was carefully applied to the sides of the "ridge" of the test object. Hence, the entire test object was insulated, except for the boiling surface itself. Two different evaporators were tested: one with a smooth surface and one with a dendritic microporous structure. The smooth surface was first machine milled, followed by manual polishing with 320p emery paper.

2.3 Test Conditions

R-134a and FC-72 were used as fluids. Saturated conditions were kept for all tests. The pressure was kept at 5 bar (15.7°C) and 0.7 bar (45.8°C) for R134a and FC-72 respectively. The chamber was evacuated to a pressure of less than 8 mbar, prior to being charged with the test liquid. Before commencing the test, the pressure (and the corresponding temperature of the test liquid) was decreased to 0.5 bar lower than the test pressure, awaiting steady state temperature conditions, and then quickly increased to the test pressure. This was done in order to reduce the vapor entrapped in the surface structure (the vapor condenses as the pressure is quickly increased when the surface is subcooled) and thereby gave all tests the same pressure history, which was important for the repeatability of the results, as reported by Gallagher and Winterton [15]. To remove air, dissolved in FC-72, the auxiliary heater was used to boil the fluid and the ventilation valve at the top of the test chamber was opened to release the uncondensed gases. The procedure was repeated, for about 2 hours, until the measured saturation pressure matched fluid data.

The heaters of the test objects were supplied with DC power from a computer controlled power supply (Instek, PSP-405). The current and voltage were measured with the power supply unit. The test series were initiated at maximum heat flux for the test series, upon which the whole surface rapidly erupted into nucleate boiling. The power input was then gradually decreased. Temperatures were sampled every second and when 20 consecutive

readings from each thermocouple were within an interval of 0.1 K, the average values of the readings were recorded and the heat flux was changed to the next measurement point. The boiling curves were reproduced twice within the accuracy of the thermocouples. To minimize heat transfer from the light sources, the lamps were only switched on during the short time of filming (0.5 – 1 s). During this short time period, no heat transfer from the lamps was measured.

2.4 Data Reduction

The heat transfer coefficient, *h*, for the different boiling surfaces was calculated according to

$$h = Q'/(A \cdot \Delta T)$$

where the heat flow rate, Q', was calculated from the voltage and current output from the power supply unit. Voltage drop over the power leads were corrected for. The apparent heat transfer area, *A*, was calculated as

$$A = wL.$$

The dimensions of the boiling surface were measured, by analyzing close-up pictures of the surface with a micrometer reference in the picture. The temperature difference, ΔT, was defined as the difference between the surface temperature, T_s, and the liquid temperature measured 10 mm above the surface, T_{liq}. A finite element solver (COMSOL) was used to model the entire test object to calculate T_s, from the average temperature measured with thermocouples in the thermocouple wells and to model heat losses from the entire test object. The difference between the calculated surface temperature and the measured temperature at the location of the thermocouple, 2 mm below the surface, was found to vary between a few hundredths (at min. heat flux) to a few tenths (at max. heat flux) of a K and was corrected for in the calculation of heat transfer coefficient. The relative heat losses through the insulation were calculated with the method presented in Furberg (2006) and were found to be inversely proportional to the heat flux. The magnitude of the heat loss was in the range of a few percent, which were accounted for in the calculation of the heat transfer coefficient.

Images from the high speed camera were used to quantify bubble size and rising velocity. As illustrated in Figure 3, from the images recorded, a 4x2.5 mm window was cropped out. This window was located 2 mm above the boiling surface to avoid the influence of the intense bubble coalescence at the surface. A 0.70 mm diameter wire, measured with a Mitutoyu micrometer (±0.01 mm), was used as a reference to determine the bubble size. The analysis was conducted by selecting one image wherein every bubble diameter was measured using image software and the average bubble velocity over the analyzed section was determined for every individual bubble. Each image contained between 20 and 300 bubbles depending on the heat flux. More bubbles at low heat flux and fewer, but larger bubbles at high heat flux. At least 3 images were analyzed at each heat flux and the variation of bubble diameter, bubble frequency density, and latent and sensible heat flux between the images at each heat flux was found to be within ± 7%, ± 16% and ± 15% respectively. With the extensive calibration and considering that temperature differences were measured, the uncertainty interval for the temperature difference (ΔT) has been estimated to ±0.1 K. The uncertainty in the surface area was calculated to ±0.3% and the power input to ± 0.2%. The width of the reference wire was determined to ± 10 µm, equivalent to 1.4%. The reproducibility of the reference wire measurement was found to be ± 0.5% and of the bubble diameter to ± 5%.

The individual bubble volume, V_i, was determined by measuring the major and minor bubble diameters, d_1 and d_2, assuming an ellipsoidal shape. The various bubble characteristics for each individual bubble, *i*, in a particular image, were calculated as follows; at steady state conditions, two sequential picture frames of the analyzed section (a given area) are representative of the average vapor flow given that there is a large enough number of bubbles included in the analyzed section. Hence, the bubble frequency for each bubble in the analyzed image, f_i, was calculated as

$$f_i = \tau^{-1}_i$$

where τ_i was the time it took for the bubble to move through the analyzed section. The average bubble frequency density, n_b, was calculated as

$$n_b = \Sigma f_i / (L_{window} w)$$

where L_{window} is the length of the analyzed section and w is the width of the boiling surface, as indicated in Figure 3. The vapor volume flow rate for each bubble, V'_i, was calculated as

$$V'_i = f_i V_i$$

Since, the bubbles in each image were assumed to be representative of the steady state condition, the heat transferred as total latent heat, Q'_{lat}, was calculated according to

$$Q'_{lat} = \rho_{sat,\,X=1} h_{fg} \Sigma V'_i$$

where $\rho_{sat,x=1}$ is the vapor saturation density at the liquid pressure. The increased vapor density inside the bubble due to surface tension around the bubble interface was calculated to less than 0.4% for the smallest bubble and was therefore neglected. h_{fg} is the enthalpy of vaporization. The average frequency weighted bubble diameter, d_{avg}, at a certain heat flux was calculated according to

$$d_{avg} = \Sigma d_i f_i \,/\, \Sigma f_i$$

where d_i is the spherical bubble diameter corresponding to V_i.

2.5 Enhanced Surface

The dendritic and microporous copper structure has previously been shown to enhance pool boiling heat coefficients in R134a with over 10 times compared to a plain, machined copper surface, Furberg et al. (2006). The enhancement structure was manufactured on the top facing surface of the test object. The structure was fabricated with an electrodeposition method where metallic copper nano-particles are dendritically connected into an ordered micro-porous structure using hydrogen bubble evolution as a dynamic masking template followed by an annealing process, as further described in Li et al. [16]. The manufacturing technique has been shown to provide ample room to control both the micro- and the nano-sized features of the surface structure, thus making changes of the geometrical dimensions of the structure possible to suit different refrigerants. For instance, larger vapor escape channels would be suitable for fluids with large liquid to vapor density ratios to facilitate effective vapor removal. Another example would be smaller wall cavities (lower wall porosity) to suit a highly wetting fluid to prevent flooding of cavities. The structure may also be applied to various geometries and in spaces of less than 2 mm.

The porous surface layer comprised a porous copper wall structure that defined and separated macro-pores, which were interconnected in the general direction normal to the surface of the substrate. The diameter of the macro-pores gradually increased with distance from the substrate and had an average top layer diameter of 105µm and a top pore density of about 75/mm^2, as seen in Figure 4. The thickness of the surface layer measured 250 µm. The porous wall consisted of dendritically shaped structures forming a large surface area and numerous cavities between its branches in the 0.1 to 1 µm range, as seen in Figure 5. The overall porosity of the surface structure was about 95%, based on the measured thickness and mass of the surface layer and the density of solid copper.

3. RESULTS AND DISCUSSION

Overall, the heat transfer performance of the test objects is higher compared to previously reported results by Furberg [11]. This is attributed to the small heater size to length scale ratio (in this case A/L), which is known to show higher levels of boiling heat transfer performance due to edge effects, as reported by Rainey and You [17]. The effect is especially pronounced for the plain reference surface, since the scale effect has a relatively greater impact on the heat transfer compared to the enhanced surface. But, since the behavior of the boiling curve and the relative improvement of the heat transfer from the enhanced surface are of the same magnitude and displaying the same trend, the general conclusions drawn from this study are thought to be applicable to larger surfaces as well.

3.1 Overall Heat Transfer Coefficients

The heat transfer coefficients for the two test surfaces and both fluids are shown in Figure 6. At any given heat flux and for both fluids, the surface temperature decreases significantly with the enhancement structure. The decrease in heat transfer coefficient in FC-72 between 10 and 15 W/cm^2 indicates that the boiling mechanism is shifting toward film boiling, or rather CHF. CHF is expected at about 15-20 W/cm^2 in boiling on a plain copper

surface in FC-72 [18, 19]. This transition does not occur for the enhancement structure, which is probably due to the separation of liquid and vapor flow in the structure [20, 21]. The vapor bubbles emerge out of the large pores that penetrate the structure top to bottom, whereas the liquid is flowing though the porous walls, probably aided by capillary forces between the fine dendritic features.

Higher absolute heat transfer performance in R134a compared to that of FC-72, can be attributed to differences in refrigerant properties that are known to affect nucleate pool boiling performance, see well known pool boiling correlations of Rohsenhow [22] and Cooper [23], such as; 20% higher thermal conductivity, 2 times larger heat of vaporization, 3 times lower molecular weight and a reduced pressure that was about 3 times higher during the tests with R134a compared to that of FC-72. Figure 7 shows the ratio of heat transfer coefficients between the enhanced and the reference surface ($h_{n\mu p}$ / h_{ref}). The ratio is decreasing with increasing heat flux for R134a. In FC-72, the ratio is not changing much with heat flux, other than at maximum heat flux where nucleate boiling regime is still present in the porous structure, but the plain surface starts to transition to film boiling, which deteriorates the heat transfer performance rapidly.

3.2 Bubble Diameter

Since the bubble diameter and frequency was measured 2 mm above the surface, the data does not exactly represent the departure diameter of bubble detaching from the surface. Visual observation from high speed photography of the surface reveals that at medium to high heat fluxes (>5W/cm^2) coalescence of bubbles from adjacent pores often takes place just prior to or after departure, but much less so at low heat flux (2 W/cm^2). As presented in Figure 8, the weighted average bubble diameter increases with heat flux for all cases, other than for the reference surface in R134a where it slightly decreases at the highest heat flux. This positive relationship between heat flux and bubble size is due to the increasing bubble coalescence that takes place as higher heat flux generates an increase in the total vapor flow. The bubble diameter from the enhanced surface was about 10 to 30% smaller for both fluids, compared to the reference surface, corresponding to about 25 to 60% smaller bubble volume.

The fact that porous surfaces tend to reduce the bubble diameter has been observed in other studies of porous enhancement structures, such as Kim et al. [24]. A number of explanations for this phenomenon may be offered. The reduction in bubble departure diameter could be a result of the high nucleation site density in the structure, resulting in early bubble coalescence of neighboring bubbles, where the resulting buoyancy force of the merged bubble is greater than the other forces keeping the bubble on the surface (i.e. surface tension, liquid inertia and bubble drag). For the plain surface, neighboring bubbles would have to grow larger before merging due to the lower nucleation site density. The significant increase in bubble coalescence at the surface of the enhanced surface at low heat flux was noticeable from the high speed videos. The convective turbulence created by the high nucleation site density could also be a contributing factor to the early bubble departure from the enhanced surface. It's also possible that the porous structure alters the contact angle and the surface tension forces acting to keep the bubble attached to the surface as suggested in the Staniszewski correlation for bubble departure diameter [25]. Further the higher nucleation site density in combination with a lower surface superheat of the enhanced surface could lead to slower bubble growth in the structure which reduces the liquid inertia forces on the bubble and thus the buoyancy forces cause the bubble to depart at smaller diameters.

3.3 Bubble Frequency Density

Visual observation from the high speed films of the boiling surfaces show that, for the reference surface, the nucleation site density is increasing noticeably with heat flux between 2-5 W/cm^2 and that especially in FC-72. On the other hand, for the enhanced surfaces, the apparent nucleation site density hardly changes for neither of the fluids and bubbles appear to be growing out of most of the visible vapor escape channels already at 2 W/cm^2. Thus, the nucleation site density is greatly enhanced and sustained by the porous structure, even at low heat flux. Figure 9 shows the bubble frequency density for both plain and enhanced surfaces in FC-72 and R134a. As seen in the high speed films of the boiling surfaces, the enhanced surface increases the bubble frequency density in both fluids, especially at low heat fluxes. This is in agreement with the visual observation from the high speed filming of the surface. The increase of active nucleation site density is consistent with the findings of other visualization studies on porous surfaces, see review by Palm [26]. Since bubble frequency and bubble diameter are related given the same latent heat flux, the possible reasons for the increase in bubble frequency are the same as those discussed in section 3.2.

Figure 9 also shows that the bubble frequency density diminishes with increasing heat flux for both surfaces and liquids. Note that the measured bubble frequency density can not be equated to the bubble departure diameter, since most bubbles have merged with another bubble at least one time, before being measured 2 mm above the

surface. The increase in bubble diameter and decrease in bubble frequency density at higher heat flux is primarily a function of increased bubble coalescence, which was visually confirmed from the videos.

3.4 Latent and Sensible Heat Flux

Figure 10 shows the calculated latent heat flux as part of the total heat flux for the plain and enhanced surfaces in both fluids. Due to the large differences in fluid properties, the proportion of the total heat transferred from the reference surface as vapor bubbles is larger for R134a than for FC-72. For both fluids, the plain surface appears to reach its maximum latent heat flux contribution at about 10 W/cm^2. The enhanced surface increases the latent heat flux contribution for both fluids by about a factor 1.2, other than at low heat flux in FC-72 where the factor is 4.5. An analysis of the high speed video images show that this large relative increase in latent heat flux in FC-72 at low heat flux is due to the low nucleation site density on the reference surface at 2 W/cm^2. Since FC-72 is a highly wetting fluid, cavities on the reference surface are easily flooded, whereas the enhanced surface apparently maintains stable nucleation points even at low heat fluxes. This was further evidenced by the data obtained on the bubble frequency density.

The total heat flux from the surface is the sum of the latent and sensible heat flux

$$q''_{tot} = q''_{lat} + q''_{sens}$$

and the overall heat transfer coefficient is defined as

$$q''_{tot} = h\Delta T$$

The latent and sensible heat flux could further be expressed as

$$q''_{lat} = h_{lat}\Delta T$$

and

$$q''_{sens} = h_{sens}\Delta T$$

where h_{lat} and h_{sens} represent the heat transfer coefficients for the latent and sensible heat flux related to the overall temperature difference between surface and bulk liquid, ΔT. Hence, the overall heat transfer coefficient could be calculated with a simple superposition model according to

$$h = h_{lat} + h_{sens}$$

Since $q''_{sens} > q''_{lat}$ for all test conditions in FC-72, it follows that $h_{sens} > h_{lat}$, which indicates that the sensible heat transfer mechanism dominates in FC-72, while the latent heat transfer mechanism governs in R134a.

The heat transfer coefficient for the enhanced surface may thus be expressed as

$$h_{n\mu p} = h_{lat\_n\mu p} + h_{sens\_n\mu p}$$

Introducing L and S as enhancement multipliers according to

$$L = h_{lat\_n\mu p} / h_{lat\_ref}$$
$$S = h_{sens\_n\mu p} / h_{sens\_ref}$$

representing the enhanced latent and sensible heat transfer coefficients caused by the porous surface structure, the heat transfer coefficient for the enhanced surface can be calculated as

$$h_{n\mu p} = L \cdot h_{lat\_ref} + S \cdot h_{sens\_ref}$$

Data shown in Figure 6 and in Figure 10 were used to calculate L and S for each data point as seen in Figure 11, L and S are between 2 and 10, which indicate that both the latent and sensible heat transfer mechanisms are significantly enhanced by the porous structure for both fluids at all heat fluxes. Two-phase enhancement (L) is mostly pronounced at lower heat flux, whereas the single-phase enhancement (S) becomes almost equally important at higher heat flux.

Enhanced latent heat transfer: The mechanisms driving the latent heat transfer take place around the liquid-, vapor- and surface interfaces of the growing vapor bubbles. That the dendritic and microporous copper structure enhanced the two-phase heat transfer mechanism 4-10 times, as seen in the *L* multiplier in Figure 11, could be attributed to some of unique features of the porous layer. As mentioned in section 3.3, bubbles appear to be growing out of most of the visible vapor escape channels in the enhanced surface even at low heat flux. Thus, the high nucleation site density even at low temperature differences is one factor explaining the large *L* multiplier at low heat flux. It is also likely that other two-phase heat transfer mechanisms are changed in the enhanced surface. Considering the large internal surface area of the dendritically shaped structure, it is possible that highly effective evaporation of thin liquid films inside the porous structure or along triple phase lines [27] account for some of the enhancement, as illustrated in Figure 12. The vapor produced within the structure must also find low impedance removal paths to prevent the formation of insulating vapor blankets within the structure. The macro-pores, which were interconnected in the general direction normal to the surface of the substrate and having a diameter gradually increasing with distance from the substrate, function as effective vapor escape channels as shown in a previous study of the structure [16].

Enhanced sensible heat transfer: Other than augmenting the bubble formation, growth and departure, the porous structure also notably enhanced the heat transfer mechanism of sensible heat 2-6 times, as seen in the *S* multiplier in Figure 11. Single phase convection is influenced by natural convection on the surface and the liquid motion caused by growing and departing bubbles. Natural convection is driven by density differences in the liquid and since the temperature difference decreases with the enhance surface, the driving force for natural convection is weaker. Even small changes in bubble formation, departure and frequency have been shown to cause significant changes of the single phase convection mechanism for a single bubble [3]. Hence, the enhanced single phase convection heat transfer could be expected to come from the strong convection caused by the agitation of the vapor bubbles inside of the porous coatings and by the increase in the number of nucleate sites. Furthermore, the copper enhancement structure itself could act as an extended surface as the liquid is moving through the highly porous walls. At higher heat fluxes and thus higher temperature differences, the enhancement caused by the enhanced single phase convection is of the same importance as the enhanced evaporation mechanism, as seen in Figure 11.

4. CONCLUSIONS

Heat transfer measurements and high speed visualization of saturated pool boiling on a dendritic and microporous copper surface in R134a and FC-72 show that, compared to that of a plain copper reference surface;

- The enhanced surface produces smaller bubbles and sustains a high bubble frequency density in both fluids, even at low heat flux.
- An enhanced latent heat transfer mechanism of up to 10 times is the main reason for the improved boiling heat transfer performance on the enhanced surface, especially at lower heat flux.
- The data also suggests that the high nucleation bubble frequency density leads to increased bubble pumping action and thus improving single phase convection of up to 6 times.
- The results in this study highlight the importance of both two and single-phase heat transfer within the porous structure. The combination of the well suited vapor escape channels, large internal area and the highly porous wall structure were features that have earlier been discussed in the conceptual mechanistic boiling model for the enhanced surface [16] that still appears to offer a plausible explanation for the enhanced boiling performance in the dendritic and microporous surface.

5. ACKNOWLEDGEMENTS

This work was supported by The Swedish Research Council for Environment, Agricultural Sciences and Spatial Planning (Formas). Thanks to Dr. Shanhua Li at the department of Functional Materials at the Royal Institute of Technology, Sweden for help with fabricating the enhanced surfaces.

REFERENCES

[1] Stephan, P., Kern, J., 2004, Evaluation of heat and mass transfer phenomena in nucleate boiling, International Journal of Heat and Fluid Flow, 25, pp. 140-148.

[2] Demiray, F., Kim, J., 2004, Microscale heat transfer measurements during pool boiling of FC-72: effect of subcooling, International Journal of Heat and Mass Transfer, 47, pp. 3257-3268.

[3] Moghaddam, S., Kiger, K., 2008. Physical mechanisms of heat transfer during single bubble nucleate boiling of FC-72 under saturated conditions – I. Experimental investigation, International Journal of Heat and Mass Transfer, 52, pp. 1284–1294.

[4] Nakayama, W., Daikoku, T., Kuwahara, H., Nakajima, T., 1980, Dynamic model of enhanced boiling heat transfer on porous surfaces, part i: experimental investigation, Journal of Heat Transfer, 102, pp. 445-450.

[5] Chen, R., Lu, M., Srinivasan, V., Wang, Z., Cho, H.H., Majumdar, A., 2009, Nanowires for enhanced boiling heat transfer, Nanoletters, 9, pp. 548-553.

[6] Ramaswamy C., Y. Joshi, W. Nakayama, W.B. Johnson, 2002, High-speed visualization of boiling from an enhanced structure, International Journal of Heat and Mass Transfer, 45, pp. 4761–4771

[7] Li, C., Peterson, G.P., 2007, Parametric study of pool boiling on horizontal highly conductive microporous coated surfaces, Journal of Heat Transfer, 129, pp.1465-1475.

[8] Kim, J., 2009, Review of nucleate pool boiling bubble heat transfer mechanisms, International Journal of Multiphase Flow, pp. 1067 – 1076.

[9] Hwang, G.-S., Kaviany, M., 2006, Critical heat flux in thin, uniform particle coatings, International Journal of Heat and Mass Transfer, 49, pp. 844-849.

[10] Furberg, R., Li. S., Palm, B., Toprak, M., Muhammed M., 2006, Dendritically ordered nano-particles in a micro-porous structure for enhanced boiling, Procedings IHTC-13 conference, Sydney, Australia, 13-18 Aug.

[11] Furberg, R., 2006, Enhanced boiling heat transfer from a novel nanodendritic micro-porous copper structure, ISSN 1102-0245, Licentiate thesis at Royal Institute of Technology, Stockholm, Sweden

[12] El-Genk, M. S, Ali, A., F., 2010, Enhanced nucleate boiling on copper micro-porous surfaces, International Journal of Multiphase Flow, 36, pp. 780–792

[13] Furberg, R., Palm, B., Li, S., Toprak, M., Muhammed, M., 2009, The use of a nano- and Microporous surface layer to enhance boiling in a plate heat exchanger, Journal of Heat Transfer, 131.

[14] Furberg, R., Li. S., Palm, B., Toprak, M., Muhammed M, 2008, Experimental investigation of an evaporator enhanced with a micro-porous structure in a two-phase thermosyphon loop, Proceedings of 2008 ASME Summer Heat Transfer Conference, HT2008, August 10-14, Jacksonville, FL, USA.

[15] Gallagher, J. P., Winterton, R. H. S., 1985, Confirmation of the pressure history theory of boiling Nucleation, Journal of Physics D: Applied Physics, 18, pp. 843-859.

[16] Li, S., Furberg, R., Toprak, M., Palm, B., and Muhammed, M., 2008, Nature-inspired fabrication of dendritic micro-porous surfaces for enhanced boiling, Advanced Functional Material, 18, pp. 2215–2220.

[17] Rainey, K. N., You, S. M., 2001, Effects of heater size and orientation on pool boiling heat transfer from microporous coated surfaces, International Journal of Heat and Mass Transfer, 44, pp. 2589-2599.

[18] O'Connor, J. P., You, S. M., 1995, A Painting technique to enhance pool boiling heat transfer in saturated fc-72, Journal of Heat Transfer, 117, pp. 387-393.

[19] El-Genk, M. S., Parker, J. L., 2005, Enhanced boiling of HFE-7100 dielectric liquid on porous graphite, Energy Conversion and Management, 46, pp. 2455-248.

[20] Liter, S. G., Kaviany, M., 2001, Pool.Boiling CHF enhancement by modulated porous-layer coating: theory and experiment, International Journal of Heat and Mass Transfer, 44, pp. 4287-4311.

[21] Mori, S., Okuyama, K., 2009, Enhancement of the critical heat flux in saturated pool boiling using honeycomb porous media, International Journal of Multiphase Flow, 35, pp. 946–951.

[22] Rohsenow, W. M., 1952, A method of correlating heat transfer data for surface boiling liquids, Transactions of ASME, 74, pp. 969-976.

[23] Cooper, M. G., 1984, Heat flow rates in saturated nucleate pool boiling—a wide ranging examination using reduced properties, Advances in Heat Transfer, Academic, Orlando, FL, pp. 203–205.

[24] Kim, J. K., Rainey, K. N., You, S. M., Pak, J. Y., 2002, Mechanism of nucleate boiling heat transfer enhancement from microporous surfaces in saturated FC-72, Journal of Heat Transfer, 124, pp. 500-506.

[25] Staniszewski B.E., 1959, Nucleate boiling bubble growth and departure, *MIT Tech.* Rep. No. 16, Cambridge, MA.

[26] Palm, B, 2009, Boiling on porous surfaces, ECI International Conference on Boiling Heat Transfer Florianópolis-SC-Brazil, 3-7 May 2009.

[27] Mitrovic, J., 2005, How to Create an Efficient Surface for Nucleate Boiling?, International Journal of Thermal Sciences, 45, pp. 1-15.

Figure 1. Schematic of test chamber

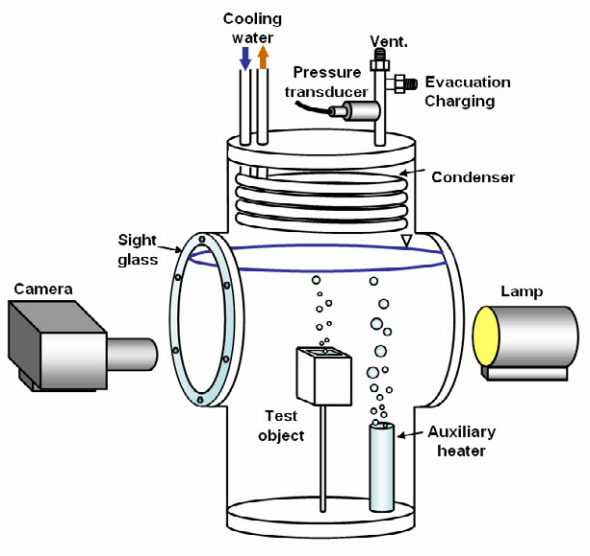

Figure 2. Schematic of test object

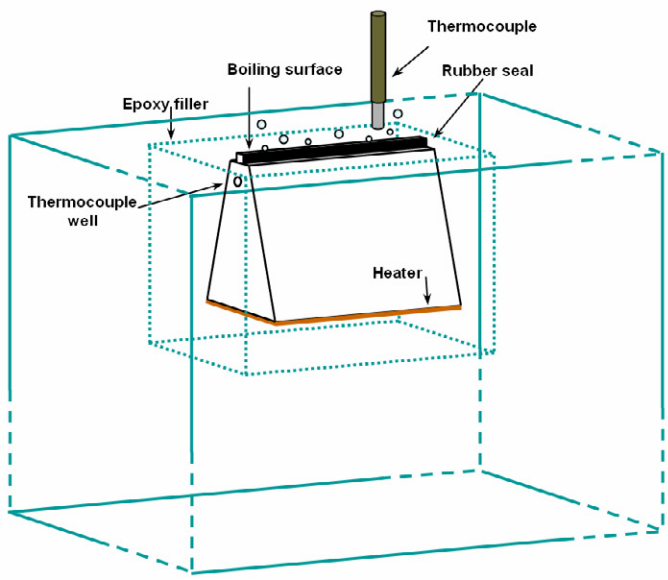

Figure 3. Filmed and analyzed sections of the boiling surface.

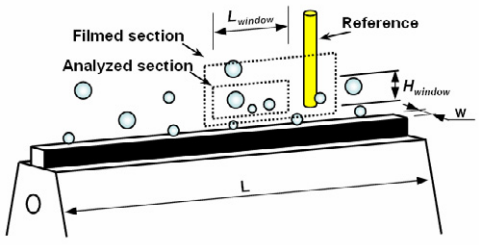

Figure 4. Top view of the boiling surface.

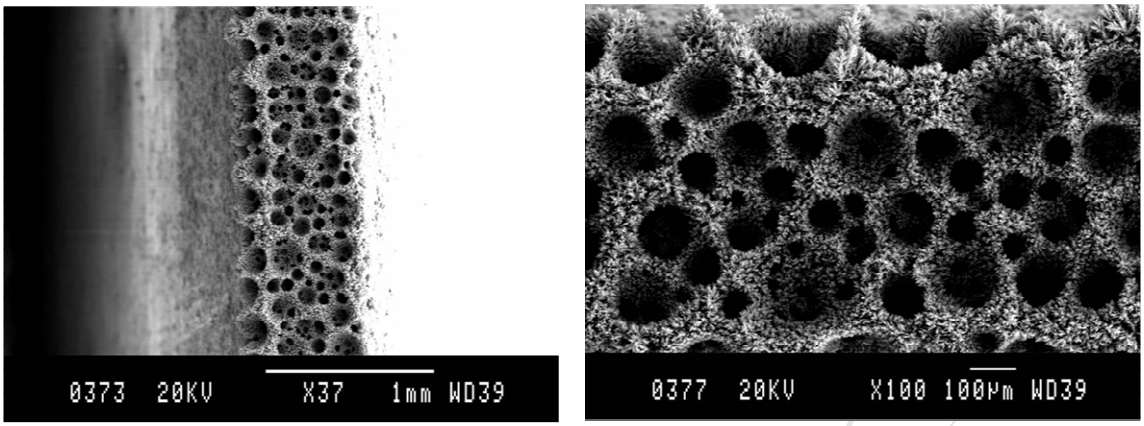

Figure 5. SEM images of the micro-porous dendritic structures

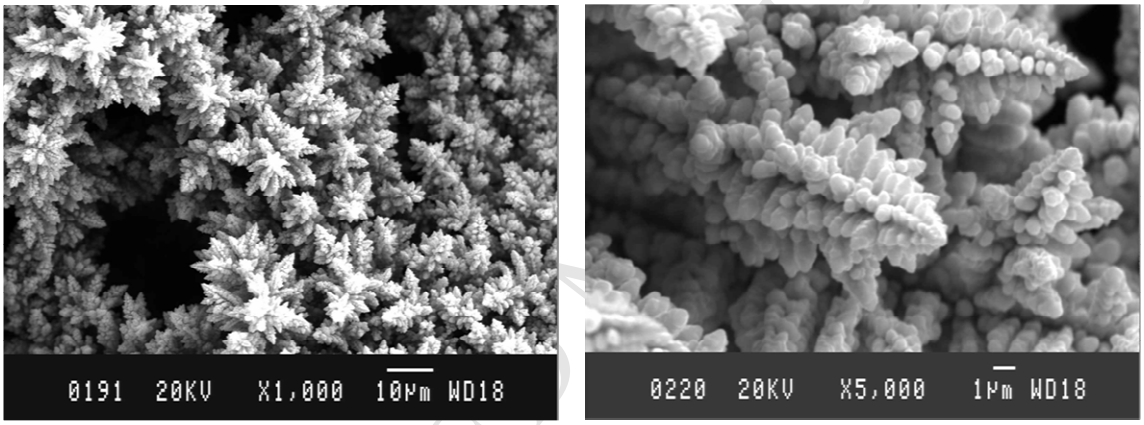

Figure 6. Heat transfer coefficients for both the plain and enhanced surface in FC-72 and R134a.

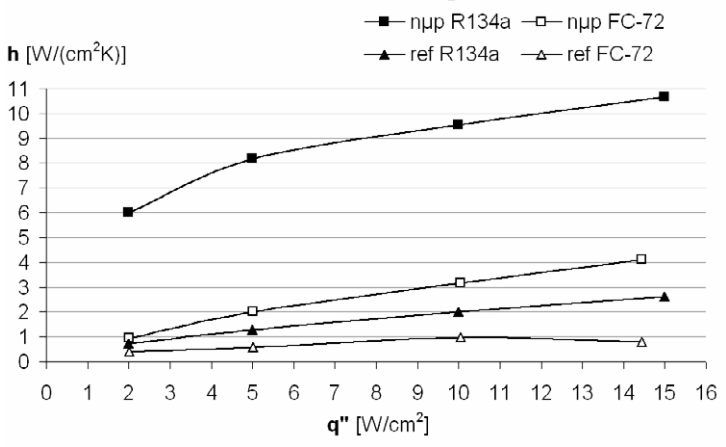

Figure 7. Ratio of heat transfer coefficients between the enhanced and the plain surface in FC-72 and R134a.

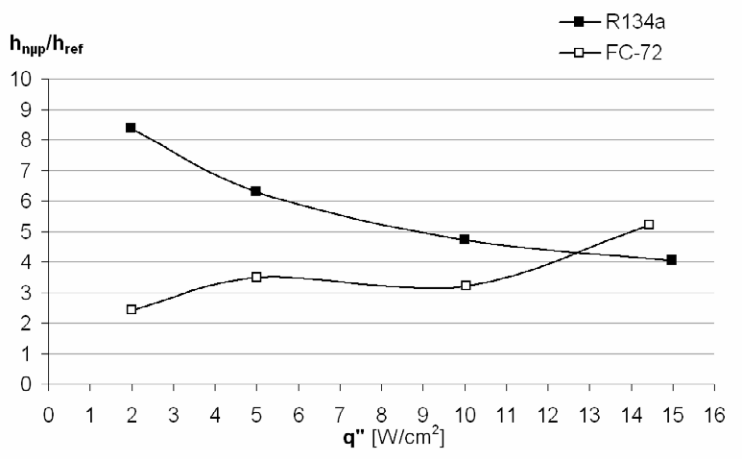

Figure 8. Average weighted bubble diameter for both plain and enhanced surfaces in FC-72 and R134a.

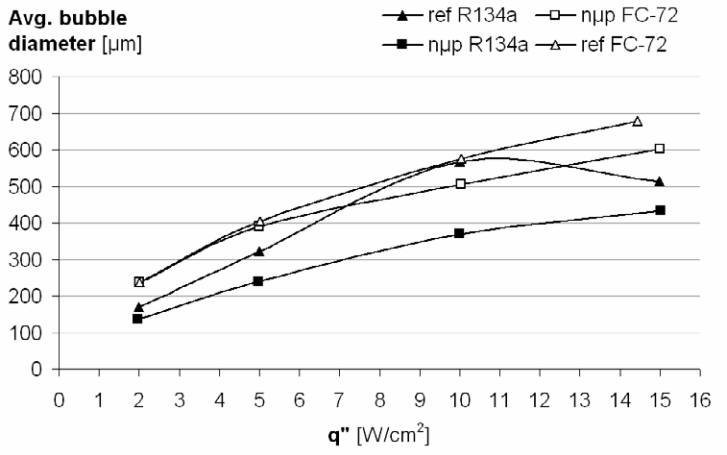

Figure 9. Bubble frequency density for both plain and enhanced surfaces in FC-72 and R134a.

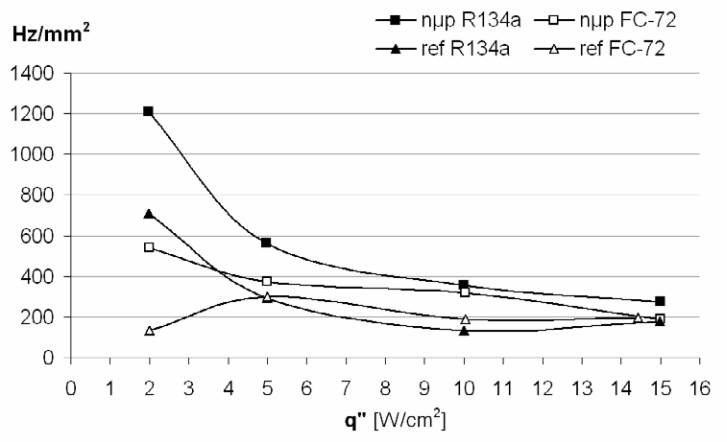

Figure 10. Latent heat flux contribution for both plain and enhanced surfaces in FC-72 and R134a.

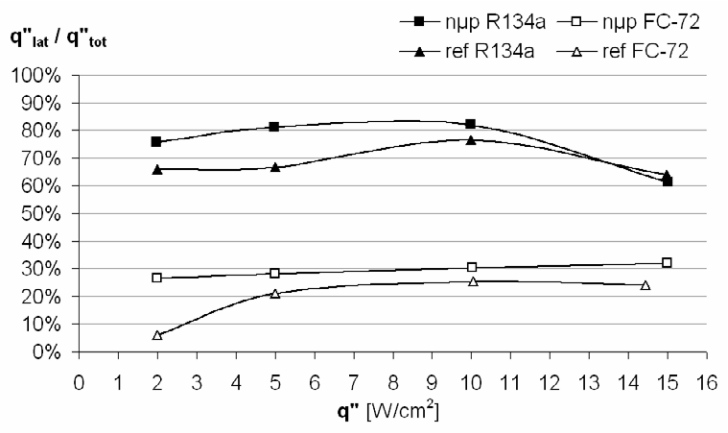

Figure 11. Enhancement multipliers, L and S, in FC-72 and R134a.

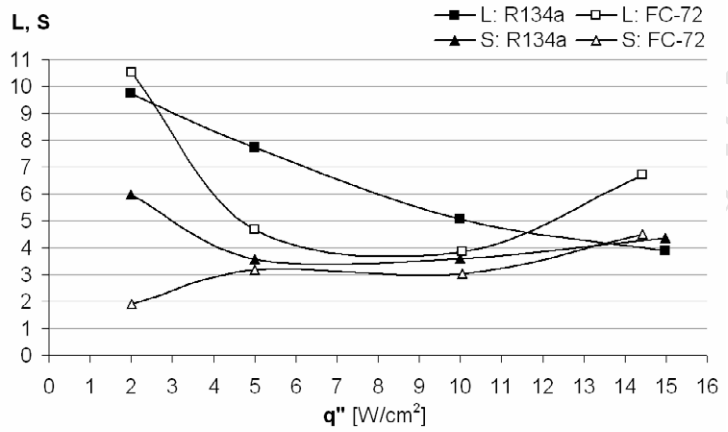

Figure 12. Simplified illustration of the enhanced structure and possible heat transfer mechanisms.

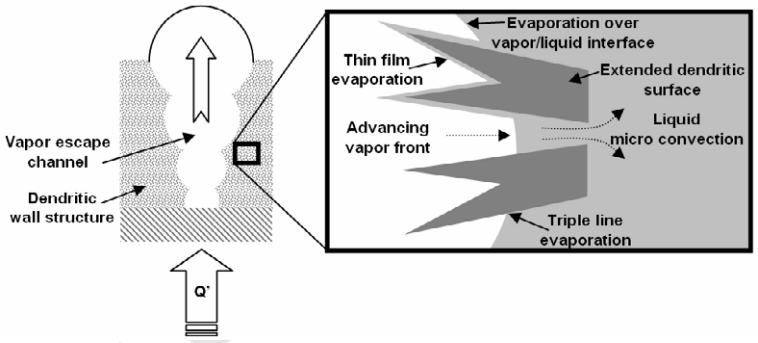

> Boiling tests on an enhanced porous surface were filmed with a high speed camera. > R134a and FC-72 were used as fluids and a plain copper surface as a reference. > The porous surface produced small bubbles at high frequency density in both fluids. > Latent and sensible heat transfer mechanisms were enhanced 10 and 6 times respectively.